

Electrochemical Oxide Growth on Nickel and Commercial Nickel Alloys: Influence of Chromium and Molybdenum

To cite this article: Isaac Kretzmer and Eric M. Stuve 2023 J. Electrochem. Soc. 170 066502

View the article online for updates and enhancements.

You may also like

- Effect of Local Cell Reaction on -NiOOH Formation in Nickel Hydrogen Battery Taichi Iwai, Shigeomi Takai and Takeshi
- The Reduction of Beta-NiOOH on the Cathode of Nickel Hydrogen Battery Due to the Local Cell Reaction Taichi Iwai, Shigeomi Takai, Takeshi Yabutsuka et al.
- Enhanced Galvanic Corrosion Phenomenon in the Welded Joint of NiCrMoV Steel by Low-Cycle Fatigue Behavior S. Weng, Y. H. Huang, F. Z. Xuan et al.







Electrochemical Oxide Growth on Nickel and Commercial Nickel Alloys: Influence of Chromium and Molybdenum

Isaac Kretzmer oz and Eric M. Stuve

Department of Chemical Engineering, University of Washington, Seattle, United States of America

Nickel-chromium-molybdenum (NiCrMo) alloys are well-known for having exceptional corrosion resistance, but their electrocatalytic properties have not been extensively studied. In this paper, the development of electro-active nickel-oxyhydroxide (NiOOH) phases and kinetics of the oxygen evolution reaction (OER) have been examined on alloys G35, B3, and C276 in alkaline electrolyte at 25 °C. Reproducible oxide layers were grown by potential cycling between 0.85 and 1.52 V vs RHE up to 600 cycles, and the transition between Ni(OH)₂ and NiOOH was monitored by cyclic voltammetry throughout. Onset potentials, Tafel slopes, and turnover frequencies (TOF) were measured at OER overpotentials between 270 and 390 mV. Alloys with dissimilar Cr:Mo ratios had significantly higher electrochemical surface area and increased γ -NiOOH formation, suggesting higher metal dissolution rates. The equal Cr:Mo concentration alloy and pure Ni developed a primarily β -NiOOH surface, and had 1.8–2.0 times larger TOF values than those containing significant γ -NiOOH. The NiCrMo alloys required smaller overpotentials (54–80 mV) to produce 10 mA cm⁻² of OER current, and had comparable Tafel slopes to pure Ni. The findings here indicate a β -NiOOH-developed surface to be more OER-active than a γ -NiOOH-developed surface, and suggest certain NiCrMo alloys have promise as OER electrocatalysts.

© 2023 The Electrochemical Society ("ECS"). Published on behalf of ECS by IOP Publishing Limited. [DOI: 10.1149/1945-7111/acd7a6]

Manuscript submitted February 2, 2023; revised manuscript received April 13, 2023. Published June 1, 2023.

The absence of efficient and affordable technologies for electricity storage hinders widespread adoption of intermittent renewable energy sources.^{1,2} Water electrolysis in alkaline media shows good potential for energy storage in the form of H₂ production. In many cases, water electrolysis is kinetically limited by the oxygen evolution reaction (OER).³ Consequently, research on OER electrocatalysts is an ongoing endeavor, with precious metal-oxides such as IrO₂ and RuO₂ being a few of the most active catalysts. Transition metals such Ni, Fe, and Co have also been studied due to their abundance and low cost.⁵ Of these, Ni-based metals are promising electrocatalysts and have been widely investigated as an electrode material due to their high electrical conductivity and resistance to corrosive alkaline environments.⁶ This makes Ni an especially attractive option for alkaline water electrolysis, as a number of studies show that Ni forms highly active oxyhydroxide species in alkaline media. 4,7–9 The Bode scheme, illustrated in Fig. 1, was first introduced in 1966 and has been extensively studied by the catalyst community through electrochemical, morphological, and spectroscopic techniques. 10-16

In alkaline media (0.1 M KOH), and in the potential range of 0 V_{RHE} to 0.5 V_{RHE}, Ni metal forms NiO and the alpha-phase hydroxide polymorph, α -Ni(OH)₂. The α -Ni(OH)₂ phase is described as turbostratic layers of Ni(OH)₂ intercalated by water molecules. 15 This phase is unstable in alkaline conditions; potentials greater than 0.5 V_{RHE} cause an irreversible transformation of α -Ni(OH)₂ to the beta-phase hydroxide polymorph β -Ni(OH)₂, the dehydrated form of α -Ni(OH)₂. ¹³ Due to the low potentials required for these reactions, formation of α -Ni(OH)₂ and subsequently β-Ni(OH)₂ happen spontaneously when exposed to alkaline media at open circuit potential, the rates of which depend on hydroxide concentration and temperature. At more positive potentials (>1.35 V_{RHE}), β -Ni(OH)₂ undergoes oxidation to its oxyhydroxide state, β -NiOOH. 14,18 This transformation is reversible, and β -NiOOH is easily reduced back to β -Ni(OH)₂. When subjected to overcharge, β -NiOOH transforms to γ -NiOOH. ¹⁵ Overcharge is loosely described as application of potentials much greater than E^{o} over prolonged periods. The value of E° is reported to be 1.33 V_{RHE} for the α -Ni(OH)₂ to γ -NiOOH transformation and 1.36 V_{RHE} for the β -Ni(OH)₂ to β -NiOOH transformation in 0.1 M KOH.¹⁹ When discharged, the gamma-phase oxyhydroxide state reduces to α -Ni(OH)₂ or β -Ni(OH)₂. Studies indicate that γ -NiOOH can also directly form from α -Ni(OH)₂ during the charging process.¹

The structure, electrochemical properties, and stability of these phases vary considerably, and the complex pathways make electrochemical investigation of the Ni oxide layer challenging.

There are some issues with using Ni as an OER electrocatalyst. It is prone to crevice corrosion attacks in chloride-containing environments, while in acidic media, dissolution of Ni is the primary concern. ^{20,21} Applying a bias to a Ni electrode can further exacerbate passivity issues. ²² An attractive alternative to pure Ni is through the use of Ni-based alloys. Chromium and molybdenum are often added to Ni in order to improve its degradation resistance through the formation of Cr(III), Mo(IV), and Mo(VI) surface oxide layers. ^{23,24} This passive film formation leads to improved breakdown potential and stability in corrosive environments. ²³ As a result, NiCrMo alloys are among the most versatile materials for a wide range of chemical and physical processes including marine environments, chlorination plants, and desulphurisation processes. ^{20–22,25}

Chromium and molybdenum modifiers for Ni electrocatalysts have been previously studied; NiCr alloys show improved alkaline urea oxidation and OER kinetics, 26,27 while NiCrMo alloys show promise for both the hydrogen evolution reaction (HER) and the ³⁰ There is good potential for NiCrMo alloys as viable alkaline electrocatalysts, but the contributions of these alloying materials are not well understood. The presence of Cr and Mo—as well as the range of applied bias—can lead to preferential formation of particular (oxy)hydroxide phases, further complicating the redox pathways presented in the Bode scheme. 31,32 In this paper, cyclic voltammetry is used to elucidate the contributions of Cr and Mo—as expressed in the commercial alloys G35, B3, and C276—to the development of NiOOH electrocatalysts on NiCrMo alloys. Potential step voltammetry, Tafel analysis, and turnover frequency are used to examine the OER kinetics on these alloys. The use of commercial alloys was motivated by their potential to serve as reference materials for studies of alkaline electrocatalysis, since their preparation is standardized by the manufacturer and is therefore independent of sample preparation protocols specific to a particular laboratory. Commercial HASTELLOY® alloys with high Cr:Mo (G35), low Cr: Mo (B3), and equal Cr:Mo (C276) ratios were supplied by Haynes International. 33

Experimental Methods

Electrochemical cell.—Aqueous KOH solution was used as the electrolyte for all electrochemical experiments and was prepared using KOH pellets (Fisher Scientific) in DI water (0.04 μ S cm⁻¹). KOH concentrations of 0.1 M (pH 13) or 1 M (pH 14) were used and

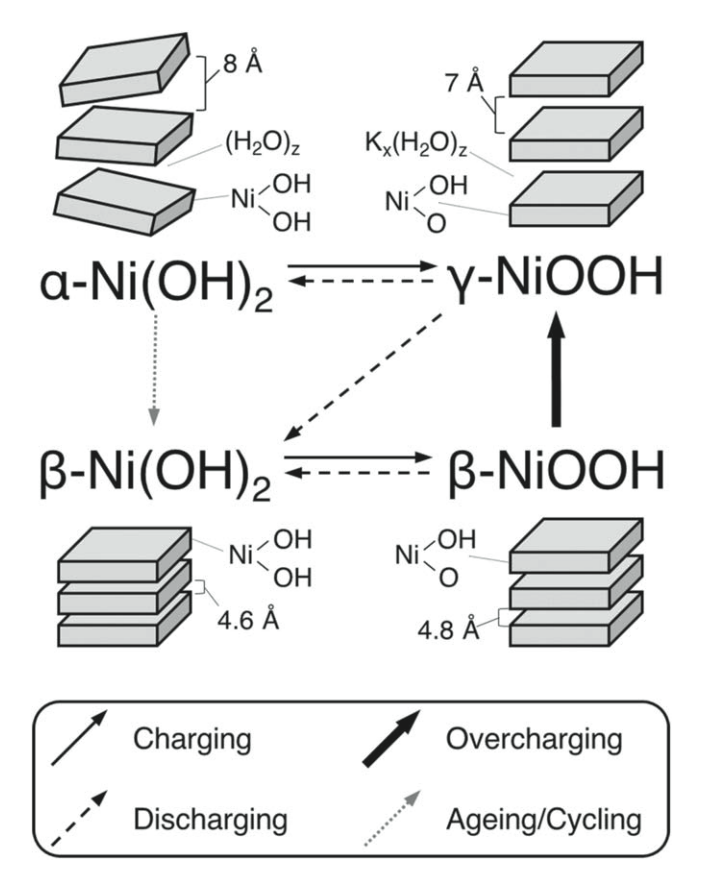


Figure 1. The general Bode scheme representation of the relationship between hydroxide and oxyhydroxide Ni surface states formed during the charge-discharge cycle in alkaline media. Adapted from Van der Ven et al.¹¹

are specified for each experiment. The KOH solution was preelectrolyzed for 1 h using two platinum electrodes to minimize solution impurities.³⁴ Argon or nitrogen gas was then sparged through the electrolyte for 20 min prior to each experiment in order to displace dissolved oxygen and create an inert environment inside the three-electrode cell (Pine Electrochemistry, 150 ml). Studies were conducted in a stagnant electrolyte, except for the potentialstep experiments which used a magnetic stir bar (200 rpm) to improve mass transfer at the electrode surface.³⁴ The temperature of the cell was set to 25 °C and controlled using a water bath and hot plate (Fisher Scientific).

Electrode preparation.—Working electrodes were made from alloys G35, B3, and C276, as well as Ni foil (0.254 mm thickness, 99.5% in purity; Alfa Aesar). The three Ni alloys were provided by Haynes International with nominal compositions shown in Table I. Prior to electrochemical studies, the electrodes were cut to size (ca. 1 cm² projected area, 2.5 cm² geometric area) using a rotary tool

Table I. Nominal compositions (wt%) for three Ni-based alloys.³³ Elements less than 1% for all alloys were excluded.

	G35	В3	C276
Ni	58	65	57
Cr	33.2	1.5	16
Mo	8.1	28.5	16
W	0.6	3	4
Co	1	3	2.5
Fe	2	1.5	5
Mn	0.5	3	1
Cr:Mo	High	Low	Equal

(Dremel 200), followed by mechanical sanding (Buehler Ecomet III). Sandpaper grits of 400, 600, 800, 1500, 3000, and 5000 were used sequentially, resulting in a smooth surface. A felt-tipped Dremel attachment and polishing compound was then used to buff the surface and remove any remaining blemishes. Finally, the electrodes were hand-polished using 1, 0.5, and 0.3 micron alumina suspension. The electrodes were sonicated in ethanol and DI water for 10 min each between each of the sanding and polishing steps. The resulting surfaces had a mirror finish that gave improved reproducibility and quality of electrochemical measurements. The counter electrode was a Pt coil (ca. 5 cm², 99.99% in purity; Pine Electrochemistry), which was also sonicated in ethanol and DI water for 10 min each prior to submersion in the electrochemical cell. An uncalibrated, single junction mercury oxide (Hg/HgO) reference electrode (4 M KOH, Pine Electrochemistry) was used due to the strong alkaline electrolyte. All subsequent unlabeled potentials will be reported with respect to the reversible hydrogen reference electrode (RHE), calculated using the following equation:

$$E_{\text{RHE}} = E_{\text{Hg/HgO}} + (0.059) \text{pH} + E_{\text{Hg/HgO}}^{\Theta}$$
 [1]

where $E_{\rm Hg/HgO}^{\Theta}$ is the standard potential of the Mercury oxide reference electrode, taken to be $+0.098~{\rm V}$ vs the normal hydrogen electrode for a 20% KOH solution at 25 °C.

Electrochemical procedures.—Electrochemical experiments were carried out using a Solartron SI 1287 potentiostat and CorrWare® for data acquisition. Once the polishing procedure and electrolyte preparation were completed, the electrode was submerged in the 0.1 M KOH (pH 13) electrolyte and subjected to a reducing potential of -0.54 V_{RHE} to remove residual oxides and surface contaminants. An electrode in this state is referred to as having an undeveloped oxide layer (UOL). To form an oxide layer, cyclic voltammograms (CV) were collected by scanning between 0.85 and 1.52 V_{RHE} at 50 mV s⁻¹, 50 times, followed by three scans in the same potential range at 1 mV s $^{-1}$. This "block" of scans was repeated 14 times for a total of 700 fast scans and 42 slow scans, leading to a developed oxide layer (DOL). After forming a DOL, the electrolyte concentration was increased to 1 M KOH (pH 14), and a potential-step experiment was conducted with 10 mV steps between 1.47-1.62 V_{RHE}, each step held for 15 min at which an approximately steady-state current was reached. The final 3 s (30 data points) for each step were averaged to reduce noise. The OER overpotential at pH 14 was calculated using an E^o of 1.23 V_{RHE}.

Results and Discussion

Oxide layer development.—Figure 2 presents the CV profiles obtained at 1 mV s⁻¹ and 25 °C in 0.1 M KOH electrolyte during the oxide development procedure for Ni, G35, C276, and B3. The voltammograms are the final scan from each block as described in the experimental section. The first and final blocks are indicated by blue and orange curves, respectively, while the gray curves show progression of the CV profiles between the first and final blocks. Due to the slow scan rate used, the amount of charging current is minimal, and the measured current can be attributed to Faradaic processes occurring at the electrode-electrolyte interface. To verify this assumption, a calculation of charging current was conducted using the following equation:³⁵

$$i_{\rm c} = AC_{\rm D}\nu \tag{2}$$

In Eq. 2, A is the surface area of the electrode (2.5 cm²), $C_{\rm D}$ the capacitance (40 μFcm^{-2}), 36 and ν is the scan rate (1 mV s⁻¹). This gives an $i_{\rm c}$ value of 0.1 μA , judged insignificant compared to the total current.

The behavior of pure Ni (Fig. 2a) initially has a single anodic (forward) peak at 1.43 V (A_1^*). This peak is generally attributed to the electrochemical transformation of β -Ni(OH)₂ to β -NiOOH and is

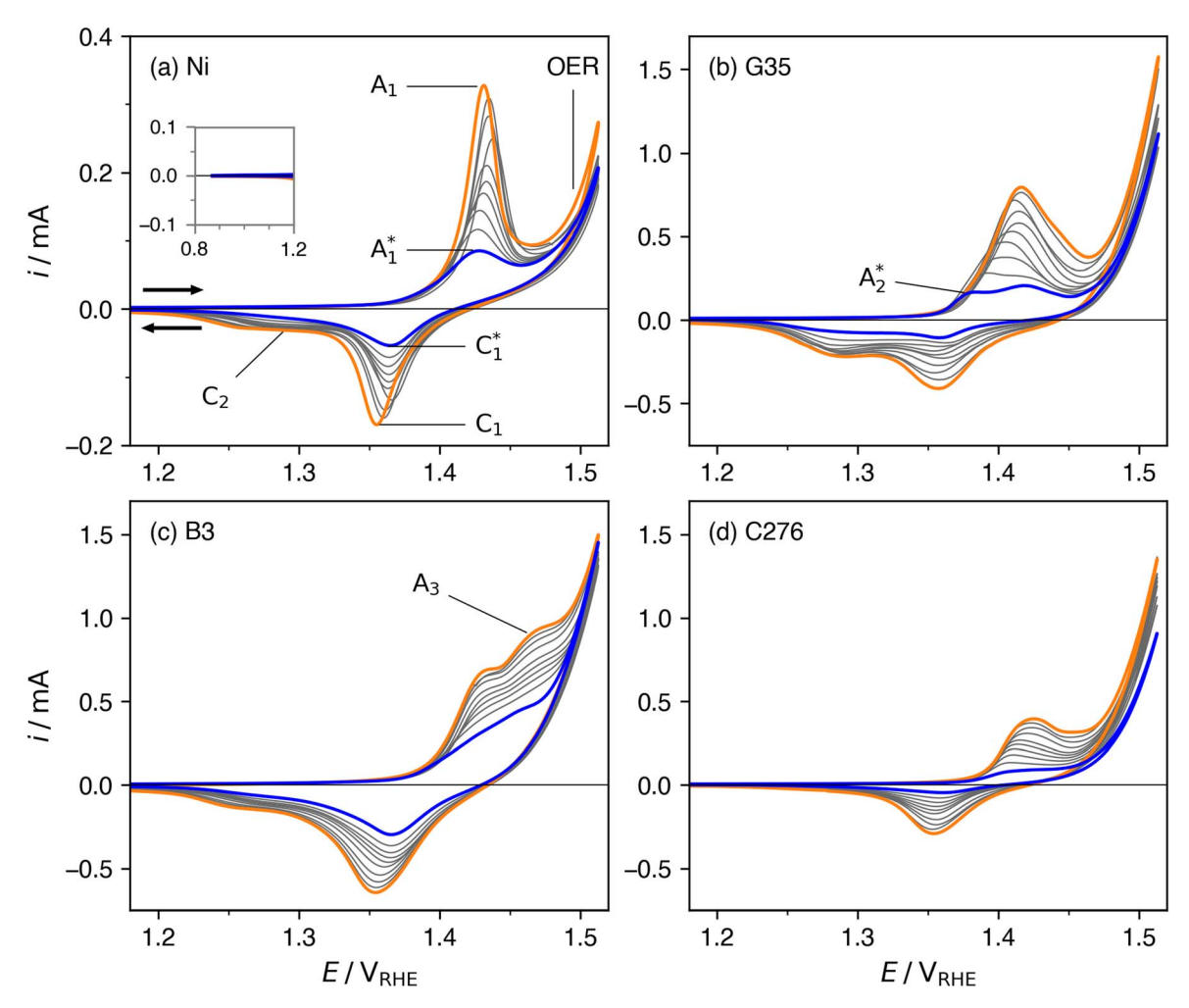


Figure 2. Cyclic voltammograms of oxide layer development procedure for (a) pure Ni, alloys (b) G35 (high Cr:Mo), (c) B3 (low Cr:Mo), and (d) C276 (equal Cr:Mo). The first block is always the smallest voltammogram and is colored blue. The final block is colored orange and is the largest. The unlabeled blocks are 2, 3, 4, 5, 6, 8, 10, and 12, and progressively increase. The electrolyte was an unstirred, 0.1 M KOH solution held at 25 °C. The inset in (a) shows the current response in the potential range of 0.80–1.2 V.

present for all electrodes. 11,13 A rise in current at more positive potentials marks the start of the OER. Although the oxygen evolution reaction has a lower standard equilibrium potential than the β -Ni(OH)₂ to β -NiOOH transformation, its sluggish kinetics requires a higher overpotential. Moreover, the generation of active β -NiOOH is crucial for OER, as the higher oxidation state assists in forming the necessary oxyhydroxide intermediates.³⁷ During the cathodic (reverse) scan, a cathodic peak at 1.37 V (C₁*) signals the electrochemical reduction of β -NiOOH to β -Ni(OH)₂. Throughout the oxide development process, peak and shoulder potentials stay relatively constant $(A_1^* \to A_1, C_1^* \to C_1)$, while the current magnitude increases. A wide, trailing shoulder between 1.32 and 1.23 V (C₂) of the cathodic scan signals the reduction of γ -NiOOH to β -Ni(OH)₂ or α -Ni(OH)₂. As the charging current in these voltammograms is minimal—and the scan rate is constant—an increase in current indicates growth in the number of active, accessible Ni sites and thus a thickening of the oxide layer.

Alloy G35 (Fig. 2b) initially has two conjoined peaks at 1.38 V and 1.42 V in the anodic scan. The less positive peak at 1.38 V (A_2^*) is attributed to the dissolution of chromium from the electrode, as similar double-peaked features have been observed for pure Cr in alkaline solutions.³⁸ The peak at 1.42 V matches that of the β -Ni(OH)₂ to β -NiOOH transition seen in pure Ni.³⁸ As the scans progress and the oxide layer develops, the β -Ni(OH)₂ to β -NiOOH peak at 1.42 V becomes the dominant voltammogram feature, fully enveloping the smaller peak by block 6. During the reverse scan, a

clear reduction peak $(\beta\text{-NiOOH} \to \beta\text{-Ni(OH)}_2)$ at 1.36 V and trailing shoulder $(\gamma\text{-NiOOH} \to \beta\text{-Ni(OH)}_2)$ or $\alpha\text{-Ni(OH)}_2)$ are initially evident. After oxide development, the shoulder has grown into a new peak at 1.29 V, while the $\beta\text{-NiOOH} \to \beta\text{-Ni(OH)}_2$ peak potential remains constant at 1.36 V.

The double-peaked cathodic scans suggest a high concentration of γ -NiOOH in the oxide layer relative to the pure Ni electrode. The formation of γ -NiOOH is generally limited by the ability to intercalate water and cations between the hydroxide layers, but accessible reaction sites may form due to passive layer dissolution. Chromium is well known to oxidize in alkaline media through the following electrochemical process: $^{23,38-40}$

$$Cr(OH)_3 + 5OH^- \rightarrow CrO_4^{2-} + 4H_2O + 3e^-$$
 [3]

The formation of transport pathways due to Cr leaching allows for the direct oxidation of α -Ni(OH)₂ to γ -NiOOH state upon charging. The increased formation of γ -NiOOH is evident by the the prominent cathodic double peak. Freshly exposed Cr sites may also contribute to the overall higher oxidation and reduction currents seen in alloy G35.

Alloy B3 (Fig. 2c) initially has no discernible peak during the forward scan, but rather a broad shoulder (1.41–1.47 V) on the leading edge of the OER curve. The shape of the reduction curve is initially similar to that of pure Ni with a peak of 1.37 V and a broad, trailing tail. During oxide development, the forward scan separates

into two distinct shoulders on the leading edge of the OER curve that plateau near E=1.43 and 1.47 V. Due to the significant overlap of these peaks with each other and the OER curve, it is difficult to discern the exact peak potentials and currents. While the shoulder at 1.43 V is presumably the β -Ni(OH) $_2$ to β -NiOOH transition, the second shoulder at 1.47 V (A $_3$) is unique to B3 and suggests the presence of an additional oxidation reaction. This feature is attributed to the electrochemical dissolution of Mo species, consistent with the high concentration of Mo in alloy B3. It has been documented that in alkaline conditions and under positive electrochemical bias, MoO $_2$ —the predominant Mo(IV) barrier species—will oxidize to form soluble Mo(VI) species: 24,25,41,42

$$MoO_2 + 2H_2O \rightarrow HMoO_4^- + 3H^+ + 2e^-$$
 [4]

Metallic Mo will also form (oxy)hydroxides, which can further oxidize to soluble Mo(VI) species:

$$Mo + 3OH^- \rightarrow Mo(OH)_3 + 3e^-$$
 [5]

$$Mo(OH)_3 + 5OH^- \rightarrow MoO_4^{2-} + 4H_2O + 3e^-$$
 [6]

Freshly exposed Mo sites on the electrode may continue to oxidize and reduce, thereby contributing to the high currents seen in alloy B3. The reduction peak shifts slightly negatively as the oxide develops, eventually stabilizing near $E_{\rm p,c}{=}1.36$ V. A trailing shoulder on this wave also forms between 1.24 and 1.30 V, indicating the presence of γ -NiOOH on the oxide surface. Similar to alloy G35, the dissolution of alloying elements may lead to an increase in accessible sites, improving the formation of γ -NiOOH.

Alloy C276 (Fig. 2d) initially has a broad wave with no discernible peak during the forward scan, but develops into a single peak with a $E_{\rm p,a}$ of 1.43 V similar to that seen in the pure Ni voltammogram. During the reverse scan, a small cathodic wave develops into a single peak at an approximately constant potential of 1.36 V. Unlike the other electrodes, there is almost no indication of γ -NiOOH on the surface. With 16% Cr and Mo concentrations, one would expect to see the formation of γ -NiOOH due to leaching as with the other alloys. An explanation for this peculiarity lies in the high Cr and Mo concentrations; according to Klapper et al.,

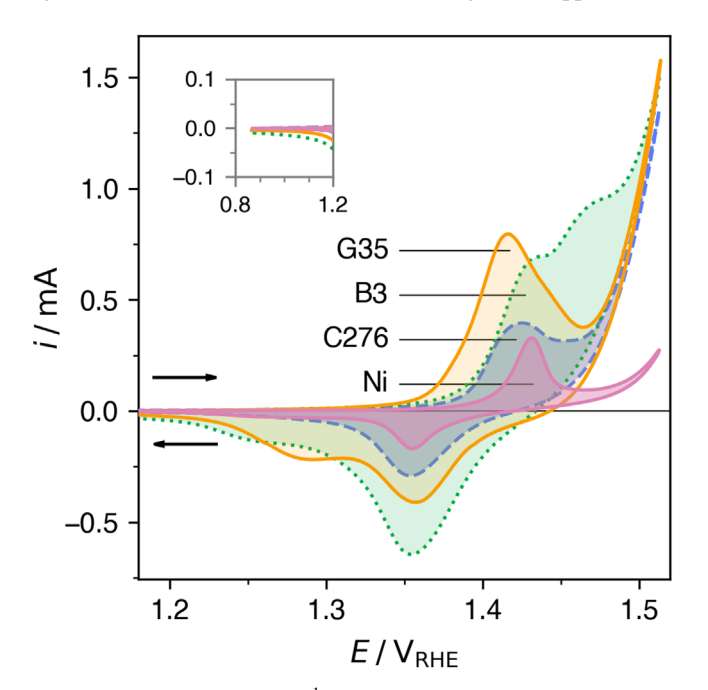


Figure 3. Third scan (1 mV s^{-1}) of the final block (14th) of the oxide development procedure for alloys G35 (high Cr:Mo), B3 (low Cr:Mo), C276 (equal Cr:Mo), and pure Ni. Inset shows the current response in the potential range of 0.80-1.2 V.

chromium has a strong influence on the crevice corrosion initiation potential, but has little effect on the repassivation behavior. 20,25 Conversely, the repassivation potential of NiCrMo alloys is determined to be a stronger function of Mo content than Cr content. A critical concentration of both elements (11% for Cr and 13% for Mo) is required for complete passivation to occur. Of the alloys studied here, only C276 meets this criteria. The implication here is that C276 undergoes minimal dissolution due to the high Cr and Mo concentrations, preventing the formation of transport pathways and inhibiting the growth of $\gamma\textsc{-NiOOH}.$

The electrochemical responses of pure Ni, G35, B3, and C276 can be summarized as follows:

- Electrochemical dissolution of Cr and Mo occurs throughout the cycling process and is most prevalent during the oxidation of Ni(OH)₂ to NiOOH.
- Freshly exposed Cr and Mo sites on the electrode contribute to the overall higher current seen in alloys G35 and B3.
- Alloying element dissolution leads to an increase in transport pathways through the oxide layer. Direct oxidation of α -Ni(OH)₂ sites and improved intercalation of cations and water increases the formation of γ -NiOOH.
- The dissolution of alloying elements and formation of γ -NiOOH is more pronounced for electrodes with dissimilar concentrations of Cr or Mo. At similar concentrations of Cr and Mo, a more stable surface layer consisting primarily of β -NiOOH is formed upon oxidation.

Voltammetry of the developed oxide layer.—Figure 3 presents the final scan block corresponding to a DOL for each of the electrodes. Values of particular interest are the onset potential $(E_{\rm on})$, the peak potentials for the anodic $(E_{\rm p,a})$ and cathodic $(E_{\rm p,c})$ scans, and the half-wave potential $(E_{\rm 1/2})$. These values are shown in Table II. $E_{\rm p,a}$ and $E_{\rm 1/2}$ could not be precisely calculated for alloy B3 due to peak overlap during the anodic scan, however it is estimated to be comparable to that of C276 due to their similar leading edges.

The onset potential is estimated by drawing a tangent from the rising current down to the x-axis, and is a measure of the minimum potential needed to oxidize Ni from Ni(OH)2 to NiOOH. Eon is negatively shifted for the alloys compared to pure Ni. Alloy G35 is shifted the most, followed by B3 and C276. A negative shift in onset potential is often attributed to improved electrical conductivity of the electrode or electrolyte, as well as cation intercalation and lattice structural differences between the alloys. 44 It has been reported that the intercalation of alkali metal ions such as K⁺ and Na⁺ between layers of Ni(OH)2 during the charging process can cause a negative shift in onset potential. This may lead to stabilization of α -Ni(OH)₂, suppressing its transformation to β -Ni(OH)₂ and favoring the formation of γ -NiOOH.¹⁹ An increase in transport pathways due to Cr and Mo leaching may lead to improved K⁺ intercalation, driving the formation of γ -NiOOH and negatively shifting the Ni(OH)2 to NiOOH redox onset potential through α -Ni(OH)₂ stabilization.

Chromium and molybdenum oxidation at potentials near the Ni(OH)₂ to NiOOH redox peaks may affect the measurement of onset potential. To account for this, examination of the peak and half-wave potentials can provide a better estimate of the characteristic Ni redox features. In this case, $E_{\rm p,a}$ acts as a marker for the overall Ni(OH)₂ to NiOOH oxidation reactions and is comparable of the electrodes. The $E^{\rm o}$ value for $\alpha - \text{Ni(OH)}_2 \rightleftarrows \gamma - \text{NiOOH}$ reaction is reported to be between 30 and 50 mV less than that of the $\beta - \text{Ni(OH)}_2 \rightleftarrows \beta - \text{NiOOH}$ reaction, meaning that the formation of even small amounts of γ -NiOOH can cause negative shifts in the peak potentials. 19 With respect to alloy G35, the larger negative shift of $E_{\rm p,a}$, as compared with the other electrodes, can be attributed to additional γ -NiOOH caused by increased surface area due to Cr dissolution.

Table II. Primary characteristic voltammogram potentials (V) for a developed oxide layer of Ni-based alloys and pure Ni. Parameters in order are the onset potential, anodic peak potential, cathodic peak potential, and half-wave potential.

	Cr:Mo	$E_{\rm on}$	$E_{\rm p,a}$	$E_{\rm p,c}$	$E_{1/2}$
Ni	NA	1.397	1.431	1.355	1.393
G35	High	1.351	1.417	1.358	1.387
В3	Low	1.367	1.43 ^a	1.355	1.39 ^a
C276	Equal	1.379	1.425	1.354	1.390

a Approximated due to significant peak overlap.

The cathodic peak potential, $E_{\rm p,c}$, is a useful benchmark for the β -NiOOH reduction reaction as there is less overlap with the γ -NiOOH peak. All of the values of $E_{\rm p,c}$ fall within a 4 mV range, indicating that, while exposed Cr and Mo may contribute to increased reduction current, there is little effect on the reduction potential of β -NiOOH. The half-wave potential $E_{1/2}$ is often used to fingerprint reversible electrochemical reactions as it is an excellent estimate of $E^{\rm o.46}$ The values for $E_{1/2}$ are comparable and have a mean of 1.39 V, which is in good agreement with reported values. ¹⁹ It should be noted that that $E_{1/2}$ values presented in Table II are calculated using the $E_{\rm p,a}$ values from the combined oxidation peak, which will lead to some discrepancy with other sources. In the case of all alloys, OER current measured at the switching potential (E_{λ}) of 1.52 V is 4–5 times larger than pure Ni.

Tafel analysis.—Figure 4 shows (a) polarization curves and (b) Tafel plots for each of the electrodes collected in 1 M KOH. Characteristic values for these plots, including the OER overpotential required to produce 10 mA cm⁻² of current (η_{10}) and Tafel (b) slopes are presented in Table III. Two overpotential ranges are designated: a low range of 270–310 mV (b_{low}) and a high range of 350–390 mV (b_{high}).

The polarization curves show an OER onset potential in the range of 1.49 to 1.52 V for all electrodes. The η_{10} values for alloys G35, B3, and C276 were 58, 80, and 54 mV lower than those for pure Ni, indicating that the alloy electrodes have increased OER kinetics. The evaluated Tafel slopes are well within range of other Ni-based electrodes seen in literature. ^47-50 For Ni, the values of $b_{\rm low}$ and $b_{\rm high}$ of 42.7 and 108 mV dec⁻¹ are reasonably close to values of 40 and 120 mV dec⁻¹ derived from a microkinetics model of OER by Shinagawa et al. ⁵¹ This particular combination of Tafel slopes results from two possible rate determining steps: ⁵¹

RDS - 1:
$$MO + OH^- \rightleftharpoons MOOH^- + e^-$$
 [7]

RDS - 2:
$$MOO^- \rightleftharpoons M + O_2 + e^-$$
 [8]

Distinguishing the exact rate-determining step would require a more thorough investigation of reaction mechanisms than presented here.

In the low overpotential range, alloys G35, C276, and Ni have comparable Tafel slopes, suggesting similar OER mechanisms and rate-determining steps. In the high overpotential range, Tafel slopes for pure Ni, G35, and C276 fall in a range encompassing the value of 120 mV dec⁻¹expected for an ideal, one-electron transfer reaction. The Tafel slope of alloy B3 is noticeably higher than for the other electrodes in both overpotential ranges, however, indicating a possible change in reaction mechanism or at least a different rate-determining step within the same mechanism. Molybdenum oxidation may also contribute to the discrepancy in Tafel slopes for alloy B3; as seen in Fig. 2c, there is significant non-OER current at potentials greater than 1.5 V, overlapping with the OER feature.

Turnover frequency.—The behavior of Ni and the alloy electrodes can also be evaluated through a turnover frequency (TOF)

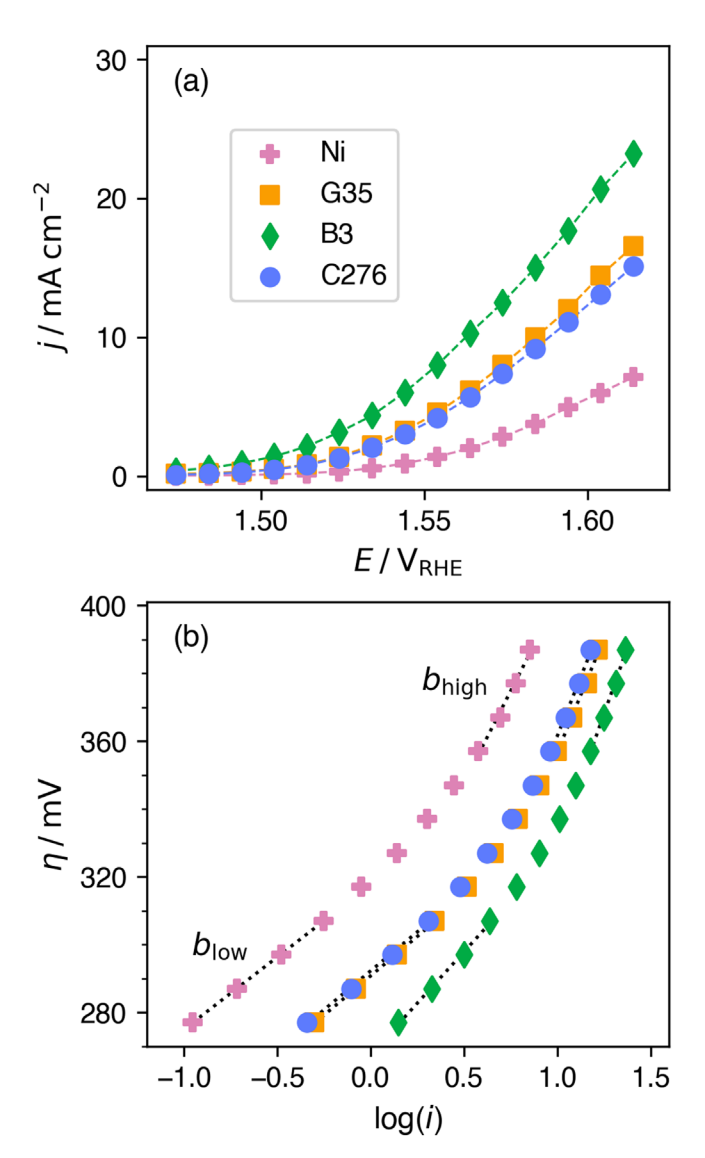


Figure 4. (a) Polarization curves and (b) Tafel plots for Ni, G35 (high Cr. Mo), B3 (low Cr:Mo), and C276 (equal Cr:Mo). Data extracted from potential step experiments. Electrolyte is 1 M KOH and stirred using a magnetic stir-bar at 200 RPM to improve mass-transfer.

analysis. This allows assessment of the accessible surface area on OER kinetics. The TOF evaluated here is based on the amount of available sites as determined by the reduction charge in the voltammograms from Fig. 3, assuming a single electron transfer process. The majority of reduction current is attributed to the reduction of β -NiOOH and γ -NiOOH, as the characteristic half wave and cathodic peak potentials are approximately the same for the alloys and pure Ni. The reduction of other alloy-specific species cannot be ruled out, however, and would require further quantitative investigation. The equation for TOF is:

$$TOF = \frac{jN_A}{nF\Gamma}$$
 [9]

where j is the OER current density, N_A is Avogadro's number, n is the number of electrons exchanged during OER (4), F is Faraday's constant, and Γ is the site density. The equation for Γ is:

$$\Gamma = \frac{q}{e} \tag{10}$$

where q is the reduction charge density found by integrating the cathodic sweep of Fig. 3, and e is the elementary charge. Turnover

Table III. Overpotential (η_{10} /mV) required to reach 10 mA cm⁻²(geometric area) and Tafel slopes (b / mV dec⁻¹) for the polarization curves presented in Fig. 4. Tafel slopes were calculated using data points in the overpotential ranges of 270–310 mV (b_{low}) and 350–390 mV (b_{high}).

	Cr:Mo	η_{10}	$b_{ m low}$	$b_{ m high}$
Ni	NA	415	42.7	108
G35	High	357	46.4	134
В3	Low	335	60.6	156
C276	Equal	361	45.9	138

frequencies were calculated for three overpotentials (300, 340, and 380 mV), which encompass the range of Tafel slope measurements.

The TOF values are presented in Fig. 5. In the low overpotential range (η_{300}), TOF values are highest for alloys C276 and B3, followed by pure Ni and G35. At η_{340} , the TOFs increase by a factor of three or more; the value for C276 is greatest, followed by pure Ni, B3, and G35. In the highest overpotential region, η_{380} , the TOFs for Ni and C276 are similar and markedly greater than those for G35 and B3. One explanation for this is the relationship between Cr:Mo ratio and γ -NiOOH formation; the electrodes with dissimilar Cr:Mo ratios (G35 and B3) have lower TOF, yet form higher concentrations of γ -NiOOH than those with similar Cr:Mo ratios (or no Cr/Mo). The implication here is that the γ -NiOOH phase has a lower TOF relative to the β -NiOOH phase, corroborating a report that the β -NiOOH phase is more active toward OER than the γ -NiOOH phase.

One final point regards the results for OER kinetics based on geometric surface area (Fig. 4) vs density of active sites (Fig. 5). Specifically, Ni and C276 require higher overpotentials for a given current density, yet exhibit higher TOFs compared to alloys G35 and B3. We interpret this along the line of total accessible surface area vs accessible oxyhydroxide sites. While exposed Cr and Mo contribute to the high electrochemical surface area of alloys G35 and B3, these alloying elements are inactive toward OER in the measured potential range. ^{53,54} As a result, the TOF values for G35 and B3 are lower than those for Ni and C276, the electrodes with less total electrochemical surface area but higher concentrations of active NiOOH sites.

Conclusions

Electrochemical oxidation and development of the oxide layer of Ni and NiCrMo alloys in alkaline electrolyte was studied as a function of potential cycling. Voltammetry, Tafel analysis, and turnover frequency were used to characterize and compare the electrocatalytic activity of the electrodes from which the following conclusions can be drawn:

- Varying the concentration of alloying elements led to preferential formation of different Ni(III) phases, but the characteristic potentials of the α -Ni(OH)₂ $\rightleftarrows \gamma$ -NiOOH and β -Ni(OH)₂ $\rightleftarrows \beta$ -NiOOH reactions were unaffected.
- Leaching of alloying elements led to an increase in transport pathways and electrochemical surface area, improving the formation of the γ -NiOOH polymorph.
- Alloys with dissimilar Cr:Mo ratios (G35, B3) had significantly higher oxidation and reduction currents than the alloy with a similar Cr:Mo ratio (C276) or pure Ni. This may be due to exposed Cr and Mo that do not dissolve, but rather continuously oxidize and reduce alongside Ni during the cycling process.
- All alloy electrodes show increased OER kinetics per geometric area relative to pure Ni, although Ni and C276 have higher and similar TOFs compared to those of G35 and B3.

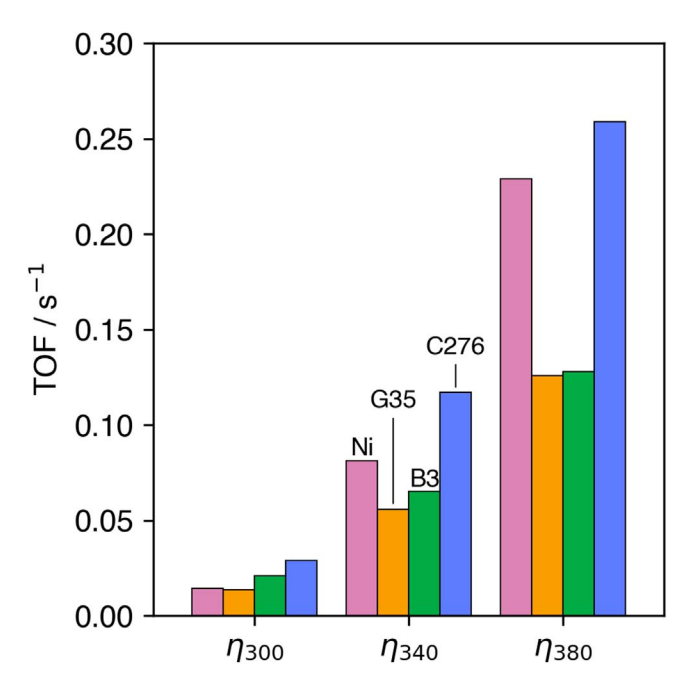


Figure 5. Calculated TOF values at overpotentials of 300, 340, and 380 mV. Bars from left to right are as follows: Pure Ni (pink), G35 (orange, high Cr. Mo), B3 (green, low Cr.Mo), and C276 (blue, equal Cr.Mo).

Acknowledgments

The authors thank Haynes International for providing materials used in this study.

Funding

Major funding was provided by the National Science Foundation [grant NSF/CBET: 2055257]. Initial support was provided by the Northwest Kidney Centers and the Center for Dialysis Innovation at the University of Washington.

ORCID

Isaac Kretzmer https://orcid.org/0000-0003-2068-3104

References

- L. Schlapbach and A. Züttel, "Hydrogen-storage materials for mobile applications." Nature, 414, 353 (2001).
- S. Ardo et al., "Pathways to electrochemical solar-hydrogen technologies." Energy & Environmental Science, 11, 2768 (2018).
- J. Song, C. Wei, Z.-F. Huang, C. Liu, L. Zeng, X. Wang, and Z. J. Xu, "A review on fundamentals for designing oxygen evolution electrocatalysts." *Chem. Soc. Rev.*, 49, 2196 (2020).
- Y. Chen, K. Rui, J. Zhu, S. X. Dou, and W. Sun, "Recent progress on Nickel-Based Oxide/(Oxy)Hydroxide electrocatalysts for the oxygen evolution reaction." Chemistry—A European Journal, 25, 703 (2019).
- M. Yu, E. Budiyanto, and H. Tüysüz, "Principles of water electrolysis and recent progress in Cobalt-, Nickel-, and Iron-based oxides for the oxygen evolution reaction." Angew. Chem. Int. Ed., 61, 3 (2022).
- ASM International, Metals Handbook Desk Edition Chapter Corrosion, p. 22 (1984)
- V. Vij, S. Sultan, A. M Harzandi, A. Meena, J. N Tiwari, W.-G Lee, T Yoon, and K. S Kim, "Nickel-based electrocatalysts for energy-related applications: oxygen reduction, oxygen evolution, and hydrogen evolution reactions." ACS Catal., 7, 7196 (2017).
- F. Song, M. M. Busch, B. Lassalle-Kaiser, C.-S. Hsu, E. Petkucheva, M. Bensimon, H. M. Chen, C. Corminboeuf, and X. Hu, "An unconventional iron nickel catalyst for the oxygen evolution reaction." ACS Central Science, 5, 558 (2019).
- K. Juodkazis, J. Juodkazytė, R. Vilkauskaitė, and V. Jasulaitiene, "Nickel surface anodic oxidation and electrocatalysis of oxygen evolution." *Journal of Solid State Electrochemistry*, 12, 1469 (2008).
- H. Bode, K. Dehmelt, and J. Witte, "Zur kenntnis der nickelhydroxidelektrode—I. Über das nickel (II)-hydroxidhydrat." *Electrochimica Acta*, 11, 1079 (1966).
- A. Van der Ven, D. Morgan, Y. S. Meng, and G. Ceder, "Phase stability of Nickel hydroxides and oxyhydroxides." J. Electrochem. Soc., 153, A210 (2006).

- P. Oliva, J. Leonardi, J. Laurent, C. Delmas, J. Braconnier, M. Figlarz, F. Fievet, and A. Guibert, "Review of the structure and the electrochemistry of nickel hydroxides and oxy-hydroxides." *Journal of Power Sources*, 8, 229 (1982).
- M. Alsabet, M. Grden, and G. Jerkiewicz, "Electrochemical growth of surface oxides on Nickel. Part 2: formation of β-Ni(OH)₂ and NiO in relation to the polarization potential, polarization time, and temperature." *Electrocatalysis*, 5, 136 (2014).
- M. Alsabet, M. Grdeń, and G. Jerkiewicz, "Electrochemical growth of surface oxides on Nickel. Part 3: formation of β-NiOOH in relation to the polarization potential, polarization time, and temperature." *Electrocatalysis*, 6, 60 (2015).
- D. S. Hall, D. J. Lockwood, C. Bock, and B. R. MacDougall, "Nickel hydroxides and related materials: a review of their structures, synthesis and properties." *Proceedings of the Royal Society A: Mathematical, Physical and Engineering Sciences*, 471, 20140792 (2015).
- D. Singh, "Characteristics and effects of γ-NiOOH on cell performance and a method to quantify it in nickel electrodes." J. Electrochem. Soc., 145, 116 (1998).
- memod to quantify it in nickel electrodess. J. Electrochem. 30c., 145, 110 (1994).
 17. M. Alsabet, M. Grden, and G. Jerkiewicz, "Electrochemical growth of surface oxides on Nickel. Part 1: formation of α-Ni(OH)₂ in relation to the polarization
- potential, polarization time, and temperature." *Electrocatalysis*, 2, 317 (2011).
 B. K. Boggs, R. L. King, and G. G. Botte, "Urea electrolysis: Direct hydrogen production from urine." *Chem. Commun.*, 45(32), 4859 (2009).
- R. Barnard, C. F. Randell, and F. L. Tye, "Studies concerning charged nickel hydroxide electrodes I. Measurement of reversible potentials." *Journal of Applied Electrochemistry*, 10, 109 (1980).
- H. S. Klapper, N. S. Zadorozne, and R. B. Rebak, "Localized corrosion characteristics of Nickel alloys: a review." *Acta Metallurgica Sinica (English Letters)*, 30, 296 (2017).
- I.-S. Forest, "The corrosion resistance of nickel-containing alloys in sulfuric acid and related compounds." *INCO The International Nickel Company*, 1, 51–82 (1983)
- L.-F. Huang, M. J. Hutchison, R. J. Santucci, J. R. Scully, and J. M. Rondinelli, "Improved electrochemical phase diagrams from theory and experiment: the Niwater system and its complex compounds." J. Phys. Chem. C, 121, 9782 (2017).
- A. C. Lloyd, J. J. Noël, S. McIntyre, and D. W. Shoesmith, "Cr, Mo and W alloying additions in Ni and their effect on passivity." *Electrochimica Acta*, 49, 3015 (2004).
- V. S. Saji and C. Lee, "Molybdenum, molybdenum oxides, and their electrochemistry." *ChemSusChem*, 5, 1146 (2012).
- A. Mishra and D. Shoesmith, "The activation/depassivation of nickel-chromium-molybdenum alloys: an oxyanion or a pH effect—Part II." *Electrochimica Acta*, 102, 328 (2013).
- R. K. Singh and A. Schechter, "Electroactivity of NiCr catalysts for urea oxidation in alkaline electrolyte." *ChemCatChem*, 9, 3374 (2017).
- J. Zhao, X. Ren, Q. Han, D. Fan, X. Sun, X. Kuang, Q. Wei, and D. Wu, "Ultra-thin wrinkled NiOOH-NiCr2O4 nanosheets on Ni foam: an advanced catalytic electrode for oxygen evolution reaction." *Chem. Commun.*, 54, 4987 (2018).
- C. González-Buch, I. Herraiz-Cardona, E. Ortega, J. García-Antón, and V. Pérez-Herranz, "Study of the catalytic activity of 3D macroporous Ni and NiMo cathodes for hydrogen production by alkaline water electrolysis." *Journal of Applied Electrochemistry*, 46, 791 (2016).
- R.-Q. Li, S. Li, M. Lu, Y. Shi, K. Qu, and Y. Zhu, "Energy-efficient hydrogen production over a high-performance bifunctional NiMo-based nanorods electrode." *J. Colloid Interface Sci.*, 571, 48 (2020).
- S. Shetty, M. Mohamed Jaffer Sadiq, D. K. Bhat, and A. C. Hegde, "Electrodeposition and characterization of Ni-Mo alloy as an electrocatalyst for alkaline water electrolysis." *Journal of Electroanalytical Chemistry*, 796, 57 (2017).
- D. E. Pissinis, L. E. Sereno, and J. M. Marioli, "Utilization of special potential scan programs for cyclic voltammetric development of different nickel oxide-hydroxide species on Ni based electrodes." J. Phys. Chem., 02, 23 (2012).
- Z. Chen, H. Deng, M. Zhang, Z. Yang, D. Hu, Y. Wang, and K. Yan, "One-step facile synthesis of nickel-chromium layered double hydroxide nanoflakes for highperformance supercapacitors." *Nanoscale Advances*, 2, 2099 (2020).
- Haynes International, Corrosion-resistant Alloys. https://haynesintl.com/alloys/ alloy-portfolio_#Corrosion-resistant-Alloys (2023).

- E. L. Clark, J. Resasco, A. Landers, J. Lin, L.-T. Chung, A. Walton, C. Hahn, T. F. Jaramillo, and A. T. Bell, "Standards and protocols for data acquisition and reporting for studies of the electrochemical reduction of carbon dioxide." ACS Catal., 8, 6560 (2018).
- A. J. Bard, L. R. Faulkner, and H. S. White, Electrochemical Methods: Fundamentals and Applications (Wiley) (2022).
- E. Cossar, M. S. Houache, Z. Zhang, and E. A. Baranova, "Comparison of electrochemical active surface area methods for various nickel nanostructures." *Journal of Electroanalytical Chemistry*, 870, 114246 (2020).
- B. S. Yeo and A. T. Bell, "In Situ Raman study of Nickel oxide and gold-supported nickel oxide catalysts for the electrochemical evolution of oxygen." *J. Phys. Chem.* C, 116, 8394 (2012).
- H. Ping, F. Hai-tao, D. Ya-ping, T. Sen, Z. Bo, and L. Wu, "Electrochemical Oxidation of Metal Chromium in odium Hydroxide Aqueous Solution." *Journal of Electrochemistry*, 26, 413 (2020).
- A. N. Colli, H. H. Girault, and A. Battistel, "Non-precious electrodes for practical alkaline water electrolysis." *Materials*, 12, 1336 (2019).
- D. Xu, M. B. Stevens, Y. Rui, G. DeLuca, S. W. Boettcher, E. Reichmanis, Y. Li, Q. Zhang, and H. Wang, "The role of Cr doping in Ni Fe oxide/(oxy)hydroxide electrocatalysts for oxygen evolution." *Electrochimica Acta*, 265, 10 (2018).
- C. R. Clayton and Y. C. Lu, "A bipolar model of the passivity of stainless steel: the role of Mo addition." J. Electrochem. Soc., 133, 2465 (1986).
- L. L. Wikstrom and K. Nobe, "The electrochemical behavior of molybdenum." J. Electrochem. Soc., 116, 525 (1969).
- J. R. Hayes, J. J. Gray, A. W. Szmodis, and C. A. Orme, "Influence of chromium and molybdenum on the corrosion of nickel-based alloys." *CORROSION*, 62, 491 (2006).
- 44. A. Mangel Raventos and R. Kortlever, "Effect of different alkali metal cations on the oxygen evolution activity and battery capacity of nickel electrodes in concentrated hydroxide electrolytes." *Electrochimica Acta*, 415, 140255 (2022).
- P. Kamath, "Suppression of the α →β-nickel hydroxide transformation in concentrated alkali: role of dissolved cations." *Journal of Applied Electrochemistry*, 31, 1315 (2001).
- E. M. Espinoza, J. A. Clark, J. Soliman, J. B. Derr, M. Morales, and V. I. Vullev, "Practical aspects of cyclic voltammetry: how to estimate reduction potentials when irreversibility prevails," J. Electrochem. Soc., 166, H3175 (2019).
- Y. Pi, Q. Shao, P. Wang, F. Lv, S. Guo, J. Guo, and X. Huang, "Trimetallic oxyhydroxide coralloids for efficient oxygen evolution electrocatalysis." *Angew. Chem.*, 129, 4573 (2017).
- S. Duan et al., "Elemental selenium enables enhanced water oxidation electrocatalysis of NiFe layered double hydroxides." *Nanoscale*, 11, 17376 (2019).
- P. Ganesan, A. Sivanantham, and S. Shanmugam, "Inexpensive electrochemical synthesis of nickel iron sulphides on nickel foam: super active and ultra-durable electrocatalysts for alkaline electrolyte membrane water electrolysis." *J. Mater. Chem. A*, 4, 16394 (2016).
- R. Sanchis-Gual, A. Seijas-Da Silva, M. Coronado-Puchau, T. F. Otero, G. Abellán, and E. Coronado, "Improving the onset potential and Tafel slope determination of earth-abundant water oxidation electrocatalysts." *Electrochimica Acta*, 388, 138613 (2021).
- T. Shinagawa, A. T. Garcia-Esparza, and K. Takanabe, "Insight on Tafel slopes from a microkinetic analysis of aqueous electrocatalysis for energy conversion." Sci. Rep., 5, 13801 (2015).
- Z. Lin, P. Bu, Y. Xiao, Q. Gao, and P. Diao, "β- and γ-NiFeOOH electrocatalysts for an efficient oxygen evolution reaction: an electrochemical activation energy aspect." J. Mater. Chem. A, 10, 20847 (2022).
- S. Anantharaj, M. Venkatesh, A. S. Salunke, T. V. S. V. Simha, V. Prabu, and S. Kundu, "High-performance oxygen evolution anode from stainless steel via controlled surface oxidation and Cr removal." ACS Sustainable Chemistry & Engineering, 5, 10072 (2017).
- R. Armstrong, M. Bell, and A. A. Metcalfe, "The anodic dissolution of molybdenum in alkaline solutions-electrochemical measurements." *Journal of Electrocanalytical Chemistry and Interfacial Electrochemistry*, 84, 61 (1977).